



ISTITUTO NAZIONALE DI RICERCA METROLOGICA Repository Istituzionale

A Three-Arm Current Comparator Digitally Assisted Bridge for the Comparison of Arbitrary Four Terminal-Pair Impedances

This is the author's accepted version of the contribution published as:

Original

A Three-Arm Current Comparator Digitally Assisted Bridge for the Comparison of Arbitrary Four Terminal-Pair Impedances / Ortolano, Massimo; D'Elia, Vincenzo; Callegaro, Luca. - In: IEEE TRANSACTIONS ON INSTRUMENTATION AND MEASUREMENT. - ISSN 0018-9456. - 66:6(2017), pp. 1496-1502. [10.1109/TIM.2016.2637458]

Availability:

This version is available at: 11696/56727 since: 2021-03-06T17:09:26Z

Publisher:

IEEE

Published

DOI:10.1109/TIM.2016.2637458

Terms of use:

This article is made available under terms and conditions as specified in the corresponding bibliographic description in the repository

Publisher copyright

IEEE

© 20XX IEEE. Personal use of this material is permitted. Permission from IEEE must be obtained for all other uses, in any current or future media, including reprinting/republishing this material for advertising or promotional purposes, creating new collective works, for resale or redistribution to servers or lists, or reuse of any copyrighted component of this work in other works

(Article begins on next page)

A three-arm current comparator digitally-assisted bridge for the comparison of arbitrary four terminal-pair impedances

Massimo Ortolano, Vincenzo D'Elia, and Luca Callegaro

Abstract—High accuracy impedance measurements are performed with coaxial transformer bridges, whose conventional design allow the comparison of like impedances — pure resistors or capacitors. Here we present a current comparator bridge suited for the measurement of impedances of arbitrary magnitudes and phase angles. The bridge has three arms, to connect the impedance under measurement and two calibrated standards. The bridge is digitally assisted and its operation is based on a polyphase digital sine wave synthesizer. To allow the measurement of mid- to low-impedance magnitudes, the bridge network and the balancing procedure are designed to approximate the four terminal-pair definition of the three impedance standards. The bridge has been extensively tested with conventional impedance standards and custom designed phase standards. The relative base accuracy is in the 10^{-5} – 10^{-6} range at kHz frequency.

Index Terms—Impedance measurement, bridge circuits, electromagnetic devices, precision measurements.

I. INTRODUCTION

Transformer impedance bridges [1]–[3] allow the measurement of the impedance ratio between two standards with ultimate accuracy at audio frequency. Such performance is based on the properties of the electromagnetic ratio devices employed, which provide voltage or current ratios very close to the nominal value and having extremely low drifts in time or versus environmental conditions [4]. The complexity of traditional transformer impedance bridges can be reduced in *digitally-assisted* bridges [3, Ch. 5] [5]–[9] which allow also automated or semi-automated operation.

The major limitation of transformer ratio bridges is that they provide a measurement only if the nominal ratio of the impedances being measured is either real (in ratio bridges) or the imaginary unit (in quadrature bridges) [3, Ch. 4].

This work presents a *three-arm*, four terminal-pair, current comparator, digitally-assisted bridge: its simple architecture allows the comparison of unlike impedances over the complex plane with a four terminal-pair definition in the audio

frequency range. To keep the number of auxiliary signals components to a minimum, the four terminal-pair definition is here approximated by nulling the *average* of the low voltage terminal-pairs (ports) of the three impedances.

A current comparator (see [10] and references therein) then combines the three admittance currents in a weighted sum, each weight being equal to the number of turns of the corresponding comparator winding. Small deviations of this sum from zero are compensated by injecting a signal generated by a digital source.

This four terminal-pair bridge has been introduced in [11] and is a development of the two terminal-pair bridge described in [12]. In the present paper we develop in detail the theory of operation, the sources of errors and we present a large selection of results.

II. PRINCIPLE OF OPERATION

A simplified schematic of the three-arm, four terminal-pair, current comparator, digitally-assisted bridge is represented in Figure 1. It is composed of the following basic elements: the voltage source E , providing the bridge excitation; the current comparator CC; three main arms containing the compared admittances Y_m , $m = 1, \dots, 3$ (for ease of notation, here and in the following sections, k denotes an index running from 0 to 3, whereas m denotes an index running from 1 to 3); the injection arm containing the voltage source E_0 which drives the admittance Y_0 ; and the synchronous detector D which senses the bridge main balance. In addition, the auxiliary voltage sources E_L and E_H , and the auxiliary detectors D_L and D_H are employed to approximate the four terminal-pair definition of the compared admittances, as described below in this Section. All sources are adjustable both in magnitude and phase. Without loss of generality, let us take admittances Y_1 and Y_2 as calibrated standards and Y_3 as the measurand. Y_0 is also a known admittance standard.

[Figure 1 about here.]

CC consists of a ferromagnetic core with high permeance \mathcal{P} , a primary winding with taps at turn numbers n_1 , n_2 and n_3 , an injection winding with turn number n_0 and a detection winding connected to D. Turn numbers are considered positive at the dotted ports, negative otherwise. The choice of turn numbers is briefly addressed in Section IV. The currents I_k , $k = 0, \dots, 3$, crossing the bridge arms produce the magnetomotive force $\mathcal{M} = \sum_{k=0}^3 n_k I_k$. The bridge is balanced when the magnetic

This activity has been partially funded by the Progetto Premiale MIUR-INRIM P6-2012, *Implementation of the new International System (SI) of Units*. The work has been carried out within the European Metrology Research Programme (EMRP) SIB 53, *Automated impedance metrology extending the quantum toolbox on electricity*. The EMRP is jointly funded by the EMRP participating countries within EURAMET and the European Union.

M. Ortolano is with the Department of Electronics and Telecommunications, Politecnico di Torino, 10129 Torino, Italy (e-mail: massimo.ortolano@polito.it).

V. D'Elia and L. Callegaro are with the Istituto Nazionale di Ricerca Metrologica (INRIM), 10135 Torino, Italy.

flux $\Phi = \mathcal{PM}$ in the comparator's core is zero, that is, when the voltage measured by D across the detection winding is zero. This condition implies $\sum_{k=0}^3 n_k I_k = 0$ and can be achieved by adjusting E_0 .

The two tracking voltage sources E_L are arranged to let the adjustment of the low voltages V_{Lm} without altering appreciably the voltage drops $V_{Hm} - V_{Lm}$, and, therefore, the currents I_m . Each low voltage V_{Lm} can be measured by connecting the synchronous detector D_L to the appropriate port.

The voltage source E_H and the synchronous detector D_H form a potentiometric arm measuring the voltage drop across the high side of the bridge, from the main excitation to each of the high-voltage ports V_{Hm} .

After applying the main excitation voltage E , the measurement procedure consists of the following steps:

- 0) Leaving unconnected the potentiometric arm composed by the source E_H and the detector D_H , set $E_L = 0$ and balance D by adjusting E_0 .
- 1) For each Y_m connect the detector D_L to the low-voltage port V_{Lm} ; adjust E_L to balance D_L , $V_{Lm} = 0$; if the main balance D changes, readjust E_0 and E_L in turns until both D and D_L are balanced; and let then E_{Lm} be the value of E_L for the admittance Y_m at the convergence of the two equilibria.
- 2) Set $E_L = (\sum_{m=1}^3 E_{Lm})/3$, to minimize the deviation of each low-voltage port from perfect four terminal-pair definition.
- 3) Recheck D and, whether necessary, readjust E_0 .
- 4) For each Y_m , connect the potentiometric arm E_H - D_H to the high-voltage port V_{Hm} ; balance D_H by adjusting E_H ; and let E_{Hm} be the value of E_H for the admittance Y_m when D_H is balanced.

To derive a practical measurement model from the above procedure, we make the assumptions below. We investigate the effect of these assumptions in Section III.

- A1) All voltage sources are ideal with zero output impedance.
- A2) The tracking between the two voltage sources E_L is perfect.
- A3) The bridge balance is not affected by small changes of E_L , that is, the currents I_m do not change appreciably during steps 1 and 2 of the measurement procedure.

From figure 1, and by assumption A3, we have $I_m = Y_m(E + E_{Lm} - E_{Hm})$ at step 1, and $I_m = Y_m(E + E_L - E_{Hm} - V_{Lm})$ at step 2. These yield $V_{Lm} = E_L - E_{Lm}$ and, by substitution, $I_m = Y_m(E + E_{Lm} - E_{Hm})$. In addition, when the bridge is balanced, $I_0 = Y_0 E_0$. With the currents I_0, \dots, I_3 thus obtained, the bridge balance equation $\sum_{k=0}^3 n_k I_k = 0$ can be solved for the unknown admittance Y_3 yielding

$$Y_3 = -\frac{n_1 Y_1 (E + E_{L1} - E_{H1}) + n_2 Y_2 (E + E_{L2} - E_{H2})}{n_3 (E + E_{L3} - E_{H3})} - \frac{n_0 Y_0 E_0}{n_3 (E + E_{L3} - E_{H3})}. \quad (1)$$

For practical calculations and for the evaluation of the uncertainty, it is more convenient to rewrite the measurement

function (1) into the following form:

$$Y_3 = -t_{13} Y_1 \frac{1 + \frac{E_{L1} - E_{H1}}{E}}{1 + \frac{E_{L3} - E_{H3}}{E}} - t_{23} Y_2 \frac{1 + \frac{E_{L2} - E_{H2}}{E}}{1 + \frac{E_{L3} - E_{H3}}{E}} - t_{03} Y_0 \frac{\frac{E_0}{E}}{1 + \frac{E_{L3} - E_{H3}}{E}}, \quad (2)$$

where we have defined the turn ratios $t_{jk} = n_j/n_k$.

Of course, the bridge can also be used to compare like impedances. In such a case, only two arms are needed (e.g., Y_1 and Y_3) and the measurement model can be simplified to determine the ratio

$$W_{13} = \frac{Z_1}{Z_3} = -t_{13} \frac{1 + \frac{E_{L1} - E_{H1}}{E} + t_{01} \frac{Y_0 E_0}{Y_1 E}}{1 + \frac{E_{L3} - E_{H3}}{E}}, \quad (3)$$

with $Z_k = 1/Y_k$.

III. ERROR SOURCES

We now drop assumptions A1–A3 of Section II. Firstly, we add a series impedance z_H to the excitation branch $E + E_L$. This impedance is crossed by the total current $I_1 + I_2 + I_3$. Then, we accept a mismatch ΔE_L between the two voltages E_L . And lastly, we assume that there is a shunt admittance Y_{Lm} at each low-voltage port. These admittances cause the equilibrium to be dependent on the low voltages V_{Lm} and generate a measurement error due to the shunt currents.

Taking into account the above conditions, the currents entering the comparator are

$$I_m = Y_m [E + E_L + \Delta E_L - E_{Hm} - V_{Lm} - z_H (I_1 + I_2 + I_3)] - V_{Lm} Y_{Lm}. \quad (4)$$

At first order, $I_1 + I_2 + I_3 \approx Y E$, with $Y = Y_1 + Y_2 + Y_3$, and $V_{Lm} \approx E_L - E_{Lm}$. Therefore,

$$I_m \approx Y_m [E + E_{Lm} - E_{Hm} + \Delta E_L - z_H Y E - (E_L - E_{Lm}) \frac{Y_{Lm}}{Y_m}]. \quad (5)$$

By substituting the currents I_m into the bridge balance equation, after some algebra we obtain

$$Y_3 = -t_{13} Y_1 \frac{1 + \frac{E_{L1} - E_{H1}}{E} + \epsilon + \epsilon_1}{1 + \frac{E_{L3} - E_{H3}}{E} + \epsilon + \epsilon_3} - t_{23} Y_2 \frac{1 + \frac{E_{L2} - E_{H2}}{E} + \epsilon + \epsilon_2}{1 + \frac{E_{L3} - E_{H3}}{E} + \epsilon + \epsilon_3} - t_{03} Y_0 \frac{\frac{E_0}{E}}{1 + \frac{E_{L3} - E_{H3}}{E} + \epsilon + \epsilon_3}, \quad (6)$$

where we have defined the error source terms

$$\epsilon = \frac{\Delta E_L}{E} - z_H Y \quad (7)$$

and

$$\epsilon_m = \frac{E_{Lm} - E_L}{E} \frac{Y_{Lm}}{Y_m}. \quad (8)$$

A Taylor series expansion of (6) yields the first-order error term

$$\Delta Y_3 = -t_{13} Y_1 (\epsilon_1 - \epsilon_3) - t_{23} Y_2 (\epsilon_2 - \epsilon_3), \quad (9)$$

which shows that ϵ has no effect at first order. This is expected because, at first order, the bridge balance is independent of the excitation voltage.

At second order, a comprehensive analysis of the error is far from straightforward because all the terms are generally complex quantities and their relative magnitude is strongly dependent on the specific experimental set-up. However, the measurement function (6) can be used on a case-by-case basis to estimate the error and to evaluate the uncertainty, possibly with the help of a numerical tool.

In the case of comparison of like impedances, equation (3) becomes

$$W_{13} = -t_{13} \frac{1 + \frac{E_{L1} - E_{H1}}{E} + \epsilon + \epsilon_1 + t_{01} \frac{Y_0 E_0}{Y_1 E}}{1 + \frac{E_{L3} - E_{H3}}{E} + \epsilon + \epsilon_3}. \quad (10)$$

IV. CURRENT COMPARATOR SETTINGS

The choice of the turn numbers n_1 , n_2 and n_3 is described in detail in [12] and is here briefly recalled. The available standards Y_1 and Y_2 and the set of available CC tap triplets $\{(n_1, n_2, n_3)\}$ define a discrete set of bridge nominal working points $Y = \{Y_3^n(n_1, n_2, n_3)\}$, with $Y_3^n(n_1, n_2, n_3) = -t_{13} Y_1 - t_{23} Y_2$, in the admittance complex plane (and the reciprocal set $Z = \{Z_3^n(n_1, n_2, n_3) = [Y_3^n(n_1, n_2, n_3)]^{-1}\}$ in the impedance plane). In other words, the admittances Y_1 , Y_2 and $Y_3^n(n_1, n_2, n_3)$ on taps n_1 , n_2 and n_3 equilibrate the bridge with null injection $I_0 \approx 0$.

When measuring a generic admittance Y_3 , better measurement accuracies are achieved for smaller injection currents I_0 , that is, close to one of the working points of the set Y . The partition of the complex admittance (impedance) plane into regions based on the distance¹ from the points of the set Y (or Z) is called *Voronoi tessellation* [13]. An example tessellation is shown in Figure 2. The best bridge setting corresponds to the region (identified by a triplet (n_1, n_2, n_3)) closer to Y_3 . In our implementation, the setting is identified by a simple program that performs an exhaustive search through all the possible triplets of turn numbers.

[Figure 2 about here.]

¹A proper definition of such a distance is given in [12].

V. EXPERIMENTAL SET-UP

The implementation of the bridge here presented is derived from the two terminal-pair version described in [12]. The coaxial schematic of the bridge is reported in Figure 3, and a photograph is shown in Figure 4.

The bridge requires for its operation a polyphase signal source with adjustable amplitude and phase for each channel. In this work we have employed two different sources:

- A 5-channel source developed at INRIM and described in [6], [7], based on a commercial digital-to-analogue (DAC) board² and filter/buffer output stages, with fine trimming of the analog gain of each channel.
- A 7-channel source developed at the University of Zielona Góra (UZG) [14], based on 18 bit digital-to-analogue converters with adjustable full scale (1 V, 2.5 V, 5 V and 10 V) and isolated precision filter/buffer output stages [15] having relative amplitude and phase stability in the 10^{-7} h^{-1} range.

The clocks of both sources are locked to the INRIM 10 MHz frequency standard.

Voltages E_L and E_H are obtained from two source output channels through 200 : 1 feedthrough injection voltage transformers [3, Sec. 3.3.9].

The current comparator CC, described in detail in [8], is wound on a toroidal amorphous ferromagnetic core. It is provided with a primary ratio winding having 21 taps corresponding to turn numbers $n = -100, -90, \dots, +90, +100$, a $n_0 = 40$ -turn balance injection winding for I_0 . The 200-turn injection winding is doubly shielded (electrostatic and magnetic shields) from the other windings.

The detector employed is a Stanford Research mod. 830 lock-in amplifier, which is manually switched across the positions D, D_L and D_H. When in position D_H, the detector is connected to the bridge through a 1 : 200 feedthrough transformer.

The adjustments of the voltages E_0 , E_{Lm} and E_{Hm} needed for the measurement procedure are done with an automatic balancing algorithm [16]. The whole measurement procedure takes around 5–10 min.

[Figure 3 about here.]

[Figure 4 about here.]

VI. MEASUREMENT RESULTS

A. Standards

The bridge implementation described in Section V has been thoroughly tested with different kind of impedances, pure and impure, in the 10Ω – $100 \text{ k}\Omega$ range. Here we report the results obtained in the range below around $10 \text{ k}\Omega$, the most interesting for what concerns four-terminal pair operation.

Table I lists the measured standards. TÜBİTAK Ulusal Metroloji Enstitüsü (UME) developed a number of resistive ratio standards and impure impedance standards, the latter to be employed as phase standards at 1 kHz. Table I also reports

²National Instruments NI-DAQ 6733 PCI Board, 16 bit resolution, 10 V full scale.

the current comparator settings n_1 , n_2 and n_3 for each set of standards.

[Table 1 about here.]

B. Uncertainty components

According to the measurement functions (6) and (10), we considered the following uncertainty components:

- Uncertainty of the calibrated admittance standards Y_1 and Y_2 , and of the injection admittance standard Y_0 . These are calibrated by comparison with the maintained national AC resistance and capacitance scales.
- Uncertainty of the turn ratios t_{jk} . Since it has not yet been possible to carry out a complete calibration of CC, the measurement results have been obtained with the nominal turn ratios. The associated uncertainty has been evaluated through a partial characterization of CC as

$$\frac{u(|t_{jk}|)}{|t_{jk}|} \approx 10^{-6} \times \max(|t_{jk}|, |t_{jk}|^{-1}) \left(\frac{f}{1000 \text{ Hz}} \right)^2, \quad (11)$$

for the magnitude, and

$$u(\arg t_{jk}) \approx 1.5 \times 10^{-6} \times \frac{f}{1000 \text{ Hz}}, \quad (12)$$

for the phase.

- Uncertainty of the voltage ratios E_0/E , E_{Lm}/E and E_{Hm}/E . Four different source channels generate the voltages E , E_0 , E_{Lm} and E_{Hm} . The voltage ratios can then be written as

$$\frac{E_0}{E} = \frac{(1 + g_0)E_0^{\text{set}}}{E}, \quad (13)$$

$$\frac{E_{Lm}}{E} = \frac{(1 + g_L)E_{Lm}^{\text{set}} + \delta V_L}{E}, \quad (14)$$

$$\frac{E_{Hm}}{E} = \frac{(1 + g_H)E_{Hm}^{\text{set}} + \delta V_H}{E}, \quad (15)$$

where the superscript *set* denotes the source settings; g_0 , g_L and g_H represent gain error terms; and δV_L and δV_H account for the balance uncertainty. The gain error terms depend on the matching between the source channels generating E_0 , E_{Lm} , E_{Hm} and the reference channel generating E , and on the accuracy of the injection transformers voltage ratio. From (14) we can infer that voltages E_{Lm} are correlated, with a correlation coefficient of about 1, because they are all generated from the same source channel, and g_L is independent of m . The same can be said for the voltages E_{Hm} , from (15). This correlation limits the contribution of the voltages E_{Lm} and E_{Hm} to the overall uncertainty. The sources employed in this experiment have channel gains matched at the 10^{-4} level, for both magnitude and phase. The balance uncertainty is better than $1 \mu\text{V}$.

- Mismatch of the E_L sources. This term is actually negligible and has not been considered.
- Effect of the excitation branch impedance z_H . In our experimental set-up, the impedance z_H can be modelled as a resistance $r_H = (70 \pm 14) \text{ m}\Omega$ in series with an inductance $l_H = (1.9 \pm 1.1) \mu\text{H}$. This impedance comprises

the source output impedance, the injection transformer impedance and the cable impedance up to node H of figure 3. Its large uncertainty accounts for possible set-up variations (e.g., the usage of two different sources).

- Effect of the shunt admittances Y_{Lm} . On the basis of our experimental set-up, we considered capacitive shunt admittances of the order of 500 pF . The term ΔY_3 has been accounted for as an uncertainty component.

The propagation of uncertainty has been carried out according to Supplement 2 of the *Guide to the expression of uncertainty in measurement* [17] with the help of `Metas.UncLib` [18].

C. Results

Tables II and III report the results obtained with the standards listed in Table I.

[Table 2 about here.]

[Table 3 about here.]

Table IV details the uncertainty budget for standard no. 13, a 30° inductive phase standard. The main uncertainty components are those associated to the reference standards Y_1 and Y_2 . The uncertainty due to the approximate definition of the low port voltages is below 10^{-6} . Table IV reports also, for comparison, the result Z_3^{ref} obtained with the three-voltmeter method³ [19]. The relative discrepancy between the two results is $(9 \pm 40) \times 10^{-6}$. Also for the other results of Table III, the main uncertainty components are those of the standards Y_1 and Y_2 , and, secondarily, that of CC. The uncertainties reported in Table III are at least one order of magnitude better than those of the best commercial *LCR* meters, and are comparable with those reported in the literature for state-of-the-art systems capable of arbitrary impedance measurements [19]–[22].

For the pure impedance standards of Table II, instead, the main uncertainty component is that of CC, especially at high turn ratios. This can be reduced through calibration.

[Table 4 about here.]

VII. CONCLUSIONS

The digitally assisted bridge here presented has two main features: i) it allows the measurement of impedances with arbitrary magnitude and phase; ii) it approximates the four-terminal pair definition of all standards with a minimal bridge network complexity. The bridge accuracy has been validated with purposely-built standards over a large range of magnitude and phase. The technique employed to achieve feature ii) is not limited to the particular bridge investigated and can be applied to other bridge networks too.

ACKNOWLEDGEMENT

The authors thank R. Rybski and J. Kaczmarek of UZG, Poland, for the development of one of the sources employed in this work, and G. Gülmez of UME, Turkey, for the development of the impure standards.

³For Z_3^{ref} , only the magnitude is reported, because the phase uncertainty of Z_3^{ref} is much greater than that of Z_3 .

REFERENCES

- [1] B. P. Kibble and G. H. Rayner, *Coaxial ac bridges*. Bristol, UK: Adam Hilger Ltd, 1984.
- [2] S. Awan, B. Kibble, and J. Schurr, *Coaxial Electrical Circuits for Interference-Free Measurements*, ser. IET Electrical Measurement. Institute of Engineering and Technology, 2010, ISBN: 9781849190695.
- [3] L. Callegaro, *Electrical impedance: principles, measurement, and applications*, ser. in Sensors. Boca Raton, FL, USA: CRC press: Taylor & Francis, 2013, ISBN: 978-1-43-984910-1.
- [4] M. E. Briggs, R. W. Gammon, and J. N. Shaumeyer, "Measurement of the temperature coefficient of ratio transformers," *Rev. Sci. Instrum.*, vol. 64, pp. 756–759, 1993.
- [5] A. C. Corney, "Digital generator-assisted impedance bridge," *IEEE Trans. Instrum. Meas.*, vol. 52, pp. 388–391, 2003.
- [6] B. Trinchera, L. Callegaro, and V. D'Elia, "Quadrature bridge for R - C comparisons based on polyphase digital synthesis," *IEEE Trans. Instrum. Meas.*, vol. 58, pp. 202–206, 2009.
- [7] L. Callegaro, V. D'Elia, and B. Trinchera, "Realization of the farad from the dc quantum Hall effect with digitally assisted impedance bridges," *Metrologia*, vol. 47, pp. 464–472, 2010.
- [8] B. Trinchera, V. D'Elia, and L. Callegaro, "A digitally assisted current comparator bridge for impedance scaling at audio frequencies," *IEEE Trans. Instrum. Meas.*, vol. 62, pp. 1771–1775, 2013.
- [9] F. Overney, F. Löönd, and B. Jeanneret, "Broadband fully automated digitally assisted coaxial bridge for high accuracy impedance ratio measurements," *Metrologia*, vol. 53, pp. 918–926, 2016.
- [10] W. J. M. Moore and P. N. Miljanic, *The current comparator*, ser. IEE electrical measurement series. London, UK: Peter Peregrinus Ltd, 1988, vol. 4, ISBN 0863411126.
- [11] M. Ortolano, V. D'Elia, and L. Callegaro, "A three-arm four terminal-pair digitally-assisted current comparator bridge for the comparison of arbitrary complex impedances," in *2016 Conference on Precision Electromagnetic Measurements (CPEM 2016)*, Ottawa, Canada, Jul. 2016.
- [12] L. Callegaro, V. D'Elia, M. Ortolano, and F. Pourdanesh, "A three-arm current comparator bridge for impedance comparisons over the complex plane," *IEEE Trans. Instrum. Meas.*, vol. 64, pp. 1466–1471, 2015.
- [13] J. Gallier, *Geometric methods and applications for computer science and engineering*, 2nd ed. New York: Springer-Verlag, 2011.
- [14] J. Kaczmarek, R. Rybski, and M. Kozioł, "The polyphase ac voltage source for digital impedance bridges," in *Final dissemination workshop of EMRP projects AIM QuTE, GraphOhm and Q-WAVE*, Prague, 18–19 May 2016. [Online]. Available: <https://www.ptb.de/emrp/sib53-finalworkshop.html>
- [15] M. Kampik, J. Torarski, M. Musioł, W. Barwinek, R. Rybski, J. Kaczmarek, M. Kozioł, and J. Nissilä, "Comparison of two buffers for impedance metrology," *Measurement Automation Monitoring*, vol. 61, no. 5, pp. 127–131, 2015.
- [16] L. Callegaro, "On strategies for automatic bridge balancing," *IEEE Trans. Instrum. Meas.*, vol. 54, pp. 529–532, 2005.
- [17] "JCGM 102:2011, Evaluation of measurement data — Supplement 2 to the "Guide to the expression of uncertainty in measurement" — Extension to any number of output quantities," 2011. [Online]. Available: <http://www.bipm.org>
- [18] M. Zeier, J. Hoffmann, and M. Wollensack, "Metas.UncLib—a measurement uncertainty calculator for advanced problems," *Metrologia*, vol. 49, p. 809, 2012.
- [19] L. Callegaro and V. D'Elia, "Automated system for inductance realization traceable to AC resistance with a three-voltmeter method," *IEEE Trans. Instrum. Meas.*, vol. 50, pp. 1630–1633, Dec 2001.
- [20] A. Muciek, "Digital impedance bridge based on a two-phase generator," *IEEE Trans. Instrum. Meas.*, vol. 46, pp. 467–470, 1997.
- [21] F. Overney and B. Jeanneret, "Realization of an inductance scale traceable to the quantum hall effect using an automated synchronous sampling system," *Metrologia*, vol. 47, pp. 690–698, 2010.
- [22] L. Callegaro, V. D'Elia, M. Kampik, D. Kim, M. Ortolano, and F. Pourdanesh, "Experiences with a two-terminal-pair digital impedance bridge," *IEEE Trans. Instrum. Meas.*, vol. 64, pp. 1460–1465, 2015.
- [23] L. Callegaro, V. D'Elia, and D. Serazio, "10-nF capacitance transfer standard," *IEEE Trans. Instrum. Meas.*, vol. 54, pp. 1869–1872, 2005.



Massimo Ortolano Massimo Ortolano was born in 1969. He received the M.Sc. degree in electronic engineering *cum laude* in 1997 from the Politecnico di Torino, Torino, Italy, and the Ph.D. degree in metrology in 2001, from the same university. Since 2000, he is an assistant professor with the Department of Electronics and Telecommunications, Politecnico di Torino, where he is in charge of several courses on electronic measurements. He collaborates with the Istituto Nazionale di Ricerca Metrologica (INRIM) on noise metrology, modelling of quantum

Hall effect devices, impedance metrology and electrolytic conductivity measurements. His research interests include also fundamental constants and time and frequency metrology.



Vincenzo D'Elia was born in 1965. He received the High School degree in electronics from the Technical School G. Plana, Turin, Italy, in 1988. After working with a telecommunication company, in 1996 he joined the Department of Electrical Metrology, Istituto Elettrotecnico Nazionale Galileo Ferraris (IEN), now Istituto Nazionale di Ricerca Metrologica (INRIM), Turin. He is currently involved in impedance, inductive voltage ratio and low current measurements.



Luca Callegaro was born in 1967. He received the degree in Electronic Engineering and the Ph.D. degree in Physics from Politecnico di Milano, Milan, Italy, in 1992 and 1996, respectively. He joined the Istituto Nazionale di Ricerca Metrologica, INRIM (formerly Istituto Elettrotecnico Nazionale Galileo Ferraris, IEN), Torino, Italy, in 1996. He has been member of the Scientific Council of IEN (1998-2005), adjunct professor of electronic measurements at Politecnico di Torino, Italy. He is responsible of research activity on electrical impedance at INRIM,

and of the national standards of electrical capacitance, inductance, ac resistance and ac voltage ratio. He is the Italian contact person of EURAMET TC-EM and member of its Working Group on Strategic Planning. He is the Italian deputy officer for the Commission A of URSI. He is author of about 70 papers on international reviews and of the book *Electrical impedance: principles, measurement and applications* (Taylor & Francis, 2012).

LIST OF FIGURES

- 1 Simplified schematic of the three-arm, four terminal-pair, current comparator, digitally-assisted bridge. The compared admittances are Y_1 , Y_2 and Y_3 . The voltage source E is the main bridge excitation. CC is the current comparator. CC's main winding has taps with turn numbers n_1 , n_2 and n_3 , counted with respect to the tap connected to E_L ; positive turn numbers are marked by black dots (in the figure above, $n_1, n_2 > 0$ and $n_3 < 0$). Currents entering the CC taps are considered positive. CC's injection winding, with turn number $n_0 < 0$, is connected to an injection arm composed of the voltage source E_0 and the admittance Y_0 . CC's detection winding is connected to the synchronous detector D, which senses the bridge main balance. The two tracking voltage sources E_L allow the adjustment of the low-voltage ports voltages V_{L1} – V_{L3} , which are measured by the synchronous detector D_L . The potentiometric arm composed by the voltage source E_H and the synchronous detector D_H is used to measure the voltage drop across the high side of the bridge. 8
- 2 A region of the Voronoi tessellation of the complex plane corresponding to the measurement no. 13 reported in Table I. The white circles represent the bridge nominal working points, which depend on the values of Y_1 and Y_2 , and on the available CC tap triplets (n_1, n_2, n_3) . The gray scale represents the magnitude of the magnetization of the current comparator generated by I_0 and needed to achieve bridge balance, relative to the total magnetization generated by I_1 , I_2 , I_3 . The red circle is the Z_3 value being measured; Z_3 falls in the region corresponding to $n_1 = -60$, $n_2 = 70$, $n_3 = -100$, as reported in the last columns of Table I. It is worth noting that Z_3 is close to the boundary between two different regions: therefore, for this particular case, the bridge setting is sensitive to the a priori knowledge of Z_3 9
- 3 Coaxial implementation of the principle schematic diagram of Figure 1. Injection/detection transformers provide voltages E_L , E_H and the detection of D_L . The black rectangles along arms 1 and 3 represent two coaxial equalizers. 10
- 4 Picture of the experimental set-up (sources and detector not shown). 11

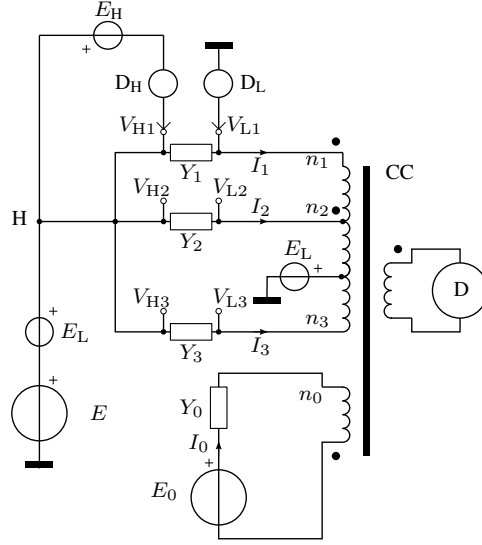


Figure 1. Simplified schematic of the three-arm, four terminal-pair, current comparator, digitally-assisted bridge. The compared admittances are Y_1 , Y_2 and Y_3 . The voltage source E is the main bridge excitation. CC is the current comparator. CC's main winding has taps with turn numbers n_1 , n_2 and n_3 , counted with respect to the tap connected to E_L ; positive turn numbers are marked by black dots (in the figure above, $n_1, n_2 > 0$ and $n_3 < 0$). Currents entering the CC taps are considered positive. CC's injection winding, with turn number $n_0 < 0$, is connected to an injection arm composed of the voltage source E_0 and the admittance Y_0 . CC's detection winding is connected to the synchronous detector D , which senses the bridge main balance. The two tracking voltage sources E_L allow the adjustment of the low-voltage ports voltages V_{L1} – V_{L3} , which are measured by the synchronous detector D_L . The potentiometric arm composed by the voltage source E_H and the synchronous detector D_H is used to measure the voltage drop across the high side of the bridge.

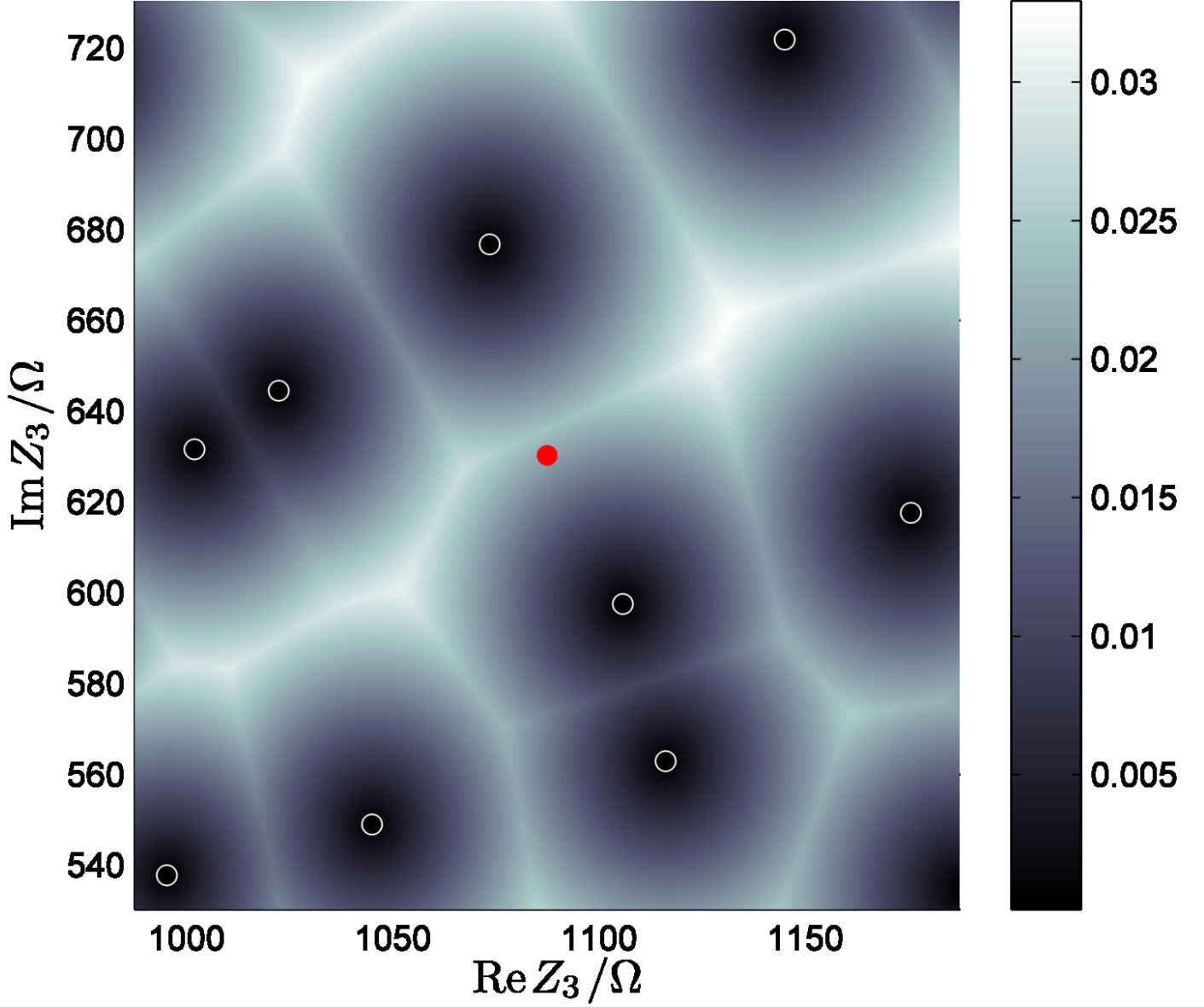


Figure 2. A region of the Voronoi tessellation of the complex plane corresponding to the measurement no. 13 reported in Table I. The white circles represent the bridge nominal working points, which depend on the values of Y_1 and Y_2 , and on the available CC tap triplets (n_1, n_2, n_3) . The gray scale represents the magnitude of the magnetization of the current comparator generated by I_0 and needed to achieve bridge balance, relative to the total magnetization generated by I_1, I_2, I_3 . The red circle is the Z_3 value being measured; Z_3 falls in the region corresponding to $n_1 = -60, n_2 = 70, n_3 = -100$, as reported in the last columns of Table I. It is worth noting that Z_3 is close to the boundary between two different regions: therefore, for this particular case, the bridge setting is sensitive to the a priori knowledge of Z_3 .

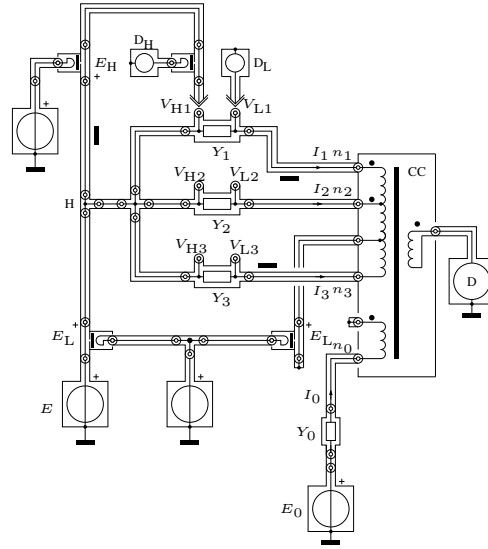


Figure 3. Coaxial implementation of the principle schematic diagram of Figure 1. Injection/detection transformers provide voltages E_L , E_H and the detection of D_L . The black rectangles along arms 1 and 3 represent two coaxial equalizers.

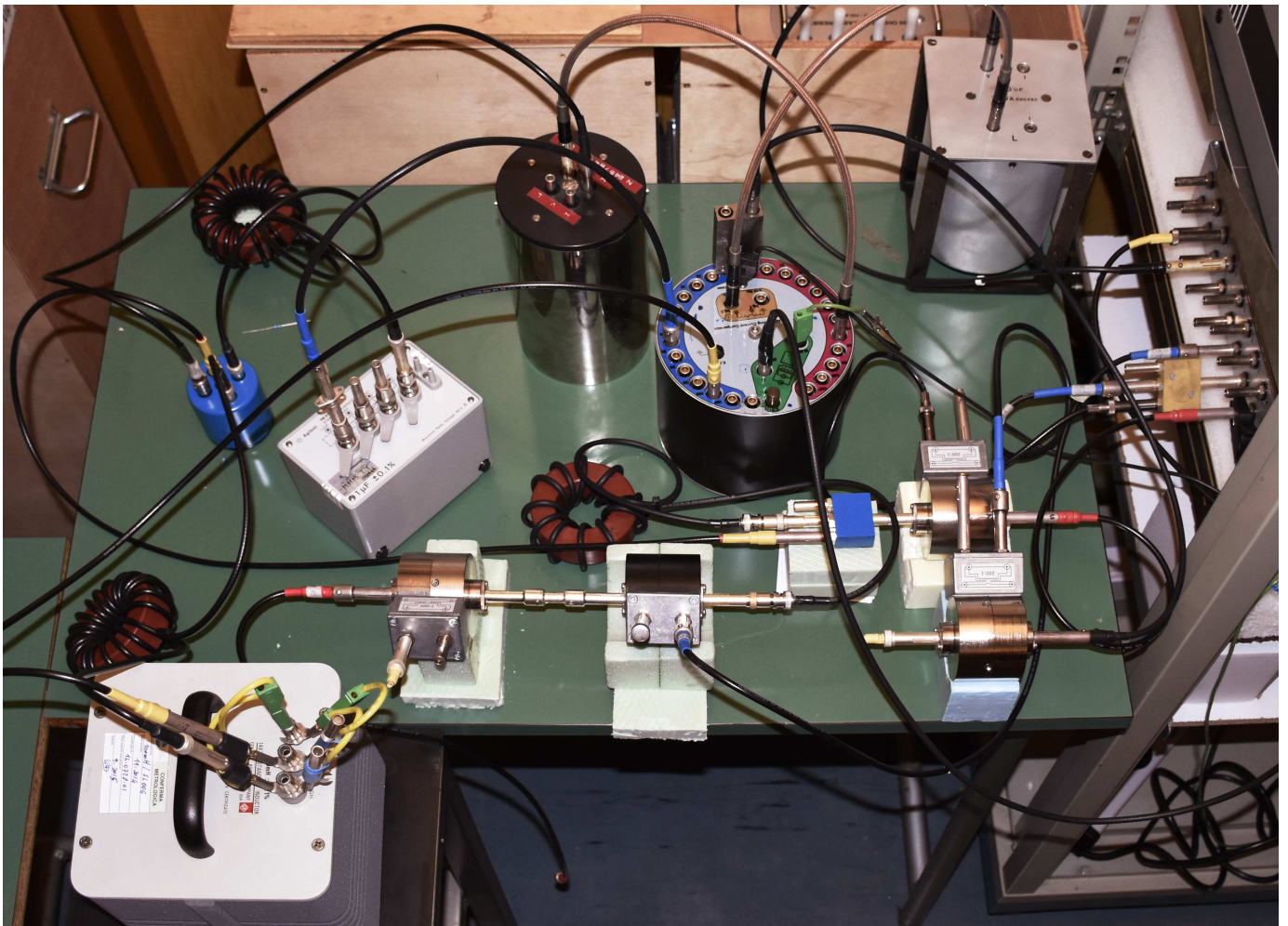


Figure 4. Picture of the experimental set-up (sources and detector not shown).

LIST OF TABLES

I	Selection of measured standards with the corresponding current comparator settings ($n_0 = -40$ for all measurements) and the excitation voltage E (RMS value). The upper part of the table lists pure impedance standards (for these, only two arms are employed, and fields Y_2 and n_2 are left empty; an asterisk * indicates that admittances Y_3 and Y_1 are part of a same ratio standard).	13
II	Results for pure impedance standards. Uncertainties are stated as standard uncertainties with a coverage factor of 1. The numbers in brackets in the fourth and sixth columns represent respectively the relative uncertainties $u(\operatorname{Re} W_{13})/ W_{13} $ and $u(\operatorname{Im} W_{13})/ W_{13} $ in parts per 10^6	14
III	Results for impure impedance standards. Uncertainties are stated as standard uncertainties with a coverage factor of 1. The numbers in brackets in the fourth and sixth columns represent respectively the uncertainties $u(Z_3)/ Z_3 $ in parts per 10^6 and $u(\arg Z_3)$ in μrad	15
IV	Uncertainty budget for measurement standard no. 13 of Table I at frequency $f = 1003.0033\text{ Hz}$. Quantities $E_{L1}-E_{L3}$, like $E_{H1}-E_{H3}$, are correlated with a correlation coefficient of 1; the propagation of uncertainty accounts for these correlations. Column nine reports the relative uncertainty components $u_i(Z_3)/ Z_3 $ in parts per 10^6 . Main uncertainty components are highlighted in bold. Type A uncertainty is negligible and has not been reported. For comparison, the last row reports the result Z_3^{ref} obtained by measuring the same standard with the three voltmeter method.	16

Table I

SELECTION OF MEASURED STANDARDS WITH THE CORRESPONDING CURRENT COMPARATOR SETTINGS ($n_0 = -40$ FOR ALL MEASUREMENTS) AND THE EXCITATION VOLTAGE E (RMS VALUE). THE UPPER PART OF THE TABLE LISTS PURE IMPEDANCE STANDARDS (FOR THESE, ONLY TWO ARMS ARE EMPLOYED, AND FIELDS Y_2 AND n_2 ARE LEFT EMPTY; AN ASTERISK * INDICATES THAT ADMITTANCES Y_3 AND Y_1 ARE PART OF A SAME RATIO STANDARD).

	Y_3	Y_2	Y_1	Y_0	n_3	n_2	n_1	E/V
Pure impedance standards								
1	TÜBITAK UME mod. 0083 1 k Ω		* 3 k Ω	Gen. Rad. mod. 3632 10 pF	30		-90	1.00
2	TÜBITAK UME mod. 0084 1 k Ω		* 7 k Ω	Gen. Rad. mod. 3632 10 pF	10		-70	1.00
3	TÜBITAK UME mod. 0086 10 k Ω		* 30 k Ω	Gen. Rad. mod. 3632 10 pF	30		-90	1.00
4	TÜBITAK UME mod. 0087 10 k Ω		* 70 k Ω	Gen. Rad. mod. 3632 10 pF	10		-70	1.00
5	Tinsley 10 Ω		INRIM (custom) 10 Ω	Towa 100 nF	50		-50	0.20
6	Tinsley 10 Ω		Tinsley 100 Ω	INRIM (custom) 10 nF	10		-100	0.20
Impure impedance standards (phase standards)								
7	TÜBITAK UME mod. 0097L 9.189 k Ω 10 nF (-30° at 1 kHz)	Tinsley 10 k Ω	IET mod. 111 10 nF	Gen. Rad. mod. 223 1 nF	90	-100	-90	0.80
8	TÜBITAK UME mod. 0098R 12.53 k Ω 22 nF (-60° at 1 kHz)	Tinsley 10 k Ω	IET mod. 111 10 nF	Gen. Rad. mod. 4127 100 pF	30	-30	-80	0.80
9	TÜBITAK UME mod. 0103L 3.62 k Ω +1 H (+60° at 1 kHz)	Tinsley 10 k Ω	IET mod. 111 10 nF	Gen. Rad. mod. 223 1 nF	-30	20	-60	0.71
10	TÜBITAK UME mod. 0103R 11.0 k Ω +1 H (+30° at 1 kHz)	Tinsley 10 k Ω	IET mod. 111 10 nF	INRIM (custom) 10 nF	-100	70	-60	0.71
11	TÜBITAK UME mod. 0104L 110 Ω +10 mH (+30° at 1 kHz)	Tinsley 100 Ω	Agilent mod. 16380C 1 μ F	INRIM (custom) 10 nF	-100	70	-60	0.10
12	TÜBITAK UME mod. 0104R 36 Ω +10 mH (+60° at 1 kHz)	Tinsley 100 Ω	Agilent mod. 16380C 1 μ F	INRIM (custom [23]) 10 nF	-30	20	-60	0.10
13	INRIM SL006 + TÜBITAK UME R1 100 mH + 1100 Ω (+30° at 1 kHz)	Tinsley 1 k Ω	Gen. Rad. mod. 1404-B 100 nF	ESI mod. SR1 1 M Ω	-100	70	-60	0.10
14	INRIM SL006 + TÜBITAK UME R2 100 mH + 362 Ω (+60° at 1 kHz)	Tinsley 1 k Ω	Gen. Rad. mod. 1404-B 100 nF	ESI mod. SR1 1 M Ω	-30	20	-60	0.10

Table II

RESULTS FOR PURE IMPEDANCE STANDARDS. UNCERTAINTIES ARE STATED AS STANDARD UNCERTAINTIES WITH A COVERAGE FACTOR OF 1. THE NUMBERS IN BRACKETS IN THE FOURTH AND SIXTH COLUMNS REPRESENT RESPECTIVELY THE RELATIVE UNCERTAINTIES $u(\operatorname{Re} W_{13})/|W_{13}|$ AND $u(\operatorname{Im} W_{13})/|W_{13}|$ IN PARTS PER 10^6 .

	f/Hz	$\operatorname{Re} W_{13}$	$\operatorname{Im} W_{13}$
1	999.9945	2.999 951 3(96) [3.2]	$-7.88(51) \times 10^{-5}$ [1.7]
2	999.9945	6.999 812(51) [7.3]	$-4.69(12) \times 10^{-4}$ [1.7]
3	399.9978	3.000 083 7(30) [1.0]	$-2.578(30) \times 10^{-4}$ [1.0]
	999.9945	3.000 083 9(96) [3.2]	$-6.473(51) \times 10^{-4}$ [1.7]
	1592.348	3.000 071(25) [7.7]	$-1.0292(76) \times 10^{-3}$ [2.5]
	1999.989	3.000 080(36) [12]	$-1.2924(93) \times 10^{-3}$ [3.1]
	4999.972	3.000 06(23) [75]	$-3.223(23) \times 10^{-3}$ [7.5]
4	999.9945	7.000 058(51) [7.3]	$-4.479(12) \times 10^{-3}$ [1.7]
5	999.9945	1.000 004 3(27) [2.7]	$6.016(60) \times 10^{-4}$ [6.0]
6	1003.0031	0.100 000 0(12) [12]	$5.050(63) \times 10^{-5}$ [6.3]

Table III

RESULTS FOR IMPURE IMPEDANCE STANDARDS. UNCERTAINTIES ARE STATED AS STANDARD UNCERTAINTIES WITH A COVERAGE FACTOR OF 1. THE NUMBERS IN BRACKETS IN THE FOURTH AND SIXTH COLUMNS REPRESENT RESPECTIVELY THE UNCERTAINTIES $u(|Z_3|)/|Z_3|$ IN PARTS PER 10^6 AND $u(\arg Z_3)$ IN μRAD .

	f/Hz	$ Z_3 /\Omega$	$\arg Z_3/^\circ$
7	999.9945	7955.938(46) [5.8]	-30.023 87(29) [5.1]
8	999.9945	5037.039(39) [7.8]	-60.438 85(47) [8.3]
9	1002.9913	7281.304(68) [9.3]	60.041 01(56) [9.8]
10	1002.9913	12 568.878(70) [5.6]	30.142 58(30) [5.3]
11	1003.0033	125.671(15) [120]	30.1359(43) [75]
12	1003.0033	72.959(10) [140]	59.813(13) [223]
13	1003.0033	1256.911(33) [26]	30.0968(18) [31]
14	1003.0033	726.189(22) [31]	60.2186(22) [38]

Table IV

UNCERTAINTY BUDGET FOR MEASUREMENT STANDARD NO. 13 OF TABLE I AT FREQUENCY $f = 1003.0033$ Hz. QUANTITIES $E_{L1}-E_{L3}$, LIKE $E_{H1}-E_{H3}$, ARE CORRELATED WITH A CORRELATION COEFFICIENT OF 1; THE PROPAGATION OF UNCERTAINTY ACCOUNTS FOR THESE CORRELATIONS. COLUMN NINE REPORTS THE RELATIVE UNCERTAINTY COMPONENTS $u_i(|Z_3|)/|Z_3|$ IN PARTS PER 10^6 . MAIN UNCERTAINTY COMPONENTS ARE HIGHLIGHTED IN BOLD. TYPE A UNCERTAINTY IS NEGLIGIBLE AND HAS NOT BEEN REPORTED. FOR COMPARISON, THE LAST ROW REPORTS THE RESULT Z_3^{ref} OBTAINED BY MEASURING THE SAME STANDARD WITH THE THREE VOLTMETER METHOD.

	Quantity	$ x_i $	$\arg x_i/\text{rad}$	$u(x_i)$	$u(\arg x_i)/\text{rad}$	Type	$u_i(Z_3)/\text{m}\Omega$	$u_i(\arg Z_3)/\mu\text{rad}$
1	Y_0	1.000 049 8 μS	0.012 579 9	6.4 pS	0.000 004 2	B	0.2 [0.2]	0.2
2	Y_1	630.260 μS	1.570 725	11 nS	0.000 042	B	22.4 [17.8]	12.4
3	Y_2	999.9248 μS	-0.000 113	1.6 nS	0.000 034	B	18.9 [15.0]	25.8
4	t_{03}	0.400 000 0	0.000 000 0	1.0×10^{-6}	0.000 001 5	B	0.1 [0.1]	0.1
5	t_{13}	0.600 000 0	0.000 000 0	1.0×10^{-6}	0.000 001 5	B	0.9 [0.7]	0.8
6	t_{23}	0.700 000 0	3.141 592 7	1.0×10^{-6}	0.000 001 5	B	1.6 [1.3]	1.3
7	E_0/E	57.8816	1.050 02	0.0058	0.000 10	B	3.7 [2.9]	2.9
8	E_{L1}/E	0.001 341 6	-2.7786	5.8×10^{-6}	0.0043	B	3.5 [2.8]	2.8
9	E_{L2}/E	0.002 129 7	-3.1174	5.8×10^{-6}	0.0027	B	6.4 [5.1]	5.1
10	E_{L3}/E	0.002 086 1	3.1336	5.8×10^{-6}	0.0028	B	7.3 [5.8]	5.8
11	E_{H1}/E	0.000 104 2	0.451	5.8×10^{-6}	0.055	B	3.5 [2.8]	2.8
12	E_{H2}/E	0.000 260 3	0.093	5.8×10^{-6}	0.022	B	6.4 [5.1]	5.1
13	E_{H3}/E	0.000 211 7	-0.210	5.8×10^{-6}	0.027	B	7.3 [5.8]	5.8
14	z_H	70.7 m Ω	0.17	7.1 m Ω	0.10	B	0.5 [0.4]	0.4
15	ΔY_3	0	0	0.67 nS	6.28	B	0.81 [0.6]	1.0
	Z_3	1256.911 Ω	0.525 291				33 [26]	31
	Z_3^{ref}	1256.898 Ω					37 [30]	